atmosphere

MDPI

Article

Climate Change and the Pattern of the Hot Spots of War in Ancient China

Shengda Zhang [1], David Dian Zhang [1,*] and Jinbao Li [2]

[1] School of Geographical Sciences, Guangzhou University, Guangzhou 510006, China
[2] Department of Geography, The University of Hong Kong, Hong Kong, China
* Correspondence: dzhang@gzhu.edu.cn

Received: 15 March 2020; Accepted: 11 April 2020; Published: 13 April 2020

Abstract: Quantitative research on climate change and war hot spots throughout history is lacking. In this study, the spatial distribution and dynamic process of war hot spots under different climatic phases in imperial China (1–1911 CE) are revealed using Emerging Hot Spot Analysis (EHSA), based on the Global Moran's Index for testing the degree of spatial autocorrelation or dependency. The results show that: (1) Battles were significantly clustered regardless of any climatic mode or war category. (2) Hot spots for all war were generally located in the Loess Plateau and the North China Plain during warm and wet periods, but in the Central Plain, the Jianghuai region, and the lower reaches of the Yangtze River/Yangtze River Delta during cold and dry conditions. (3) Hot spots for agri-nomadic conflict have similar patterns as those for all war, whereas rebellion hot spots expanded outward during warm and wet intervals yet contracted inward during cold and dry stages. These findings, by providing insightful evidence into the spatiotemporal patterns of war under the movements of climatic-ecological zones and geopolitical variations in ancient China, can be a starting point for future exploration of the long-term relationship between climate change and social security.

Keywords: climate change; war; imperial China; Global Moran's *I*; Emerging Hot Spot Analysis

1. Introduction

The climate–war nexus in historical China has been widely addressed by academic communities over the past decade [1–19]. Scientists have mostly focused on this nexus from a temporal or time-series angle, whereas the spatiality of war and its connection with climate change has rarely been investigated. Recently, our group determined that in imperial China, (1) geopolitical variables, such as the boundary between agriculturalists and pastoralists, size of agricultural empire, battle location, and the direction of war, were affected by multi-centennial precipitation fluctuation [15]; (2) the distributions of natural disasters (flood and drought) and their social impacts (famine, cannibalism, and war) were influenced by population on provincial and decadal scales [20]; and (3) secular temperature variation fundamentally regulated the spatial disparities of war via controlling agricultural and pastoral productivity [21]. However, research on the spatiotemporal pattern and its dynamic process of war has not been fully conducted.

In this study, we aimed to solve this problem by examining the linkage between climate change and the focus (or hot spot) of war in imperial China. Using the comprehensive official history and well-preserved local and private records in China since ancient times, a few native scholars have discovered the focus (similarly, geographical pivot, or strategic area) of war. For example, Song [22] divided wars in the imperial era into frontier and interior wars, and the pivots of the latter were distributed in the western Henan Corridor, the south of the Huai River (also known as the Jianghuai region), and Jing–Xiang (present-day northern Hubei). Rao [23] introduced an irregular chessboard pattern of war from a military geographical view, in which there were nine strategic areas—four

corners: Guanzhong, Hebei, Southeast China, and Sichuan; four foci/pivots: Shanxi, Shandong, Hubei, and Hanzhong; as well as the heartland, the Central Plain. Wang [24] extracted information on the spatial distribution and the shift of the focus area of war from poems in 618–765 CE (i.e., the early Tang dynasty), which implied the potential value of classic literature. Leng [25] looked into the frontier conflicts between the central governments and northern minorities during the imperial age and found that the focus areas had moved from the Hetao region and the Hexi Corridor of Northwest China since the Qin and Han dynasties to the Sixteen Prefectures of Yanyun and the western Liaoning Corridor of Northeast China after the Tang dynasty. These findings, however, are all qualitative and do not contain any climatic variables.

To fill in the research gaps, the technique in ArcMap, Emerging Hot Spot Analysis (EHSA), was applied in this study. Developed by the Environmental Systems Research Institute, Inc. (ESRI), EHSA identifies the spatial trends and distributions of different types of hot spots from data points. It has been employed by some experts to unveil spatial patterns with time, such as detecting public sentiment from geotagged photo collections in San Francisco in 2006–2015 and showing that different emotions (anger, disgust, fear, joy, sadness, and surprise) have distinct spatial distributions [26], as well as the spatiotemporal associations between a community greening program and neighborhood crime rates in Flint, Michigan, in 2005–2014 [27]. Other examples include the spatiotemporal analysis of changes in lode mining claims around the McDermitt Caldera, northern Nevada, and southern Oregon, in 1976–2010 [28], the expected trend in the occurrence of pulmonary tuberculosis cases from Hamadan Province, Iran, during 2005–2013 [29], spatial patterns of crimes (larceny and aggravated assault) in Miami-Dade County, Florida, from 2007 to 2015 [30], and statistically significant temporal-spatial trends of forest loss in Brazil, Indonesia, and the Democratic Republic of Congo between 2000 and 2014 [31]. Thus, by integrating time and space domains, EHSA was suitable for the task of uncovering the hot spots of war in China from 1 to 1911 CE. Compared with the aforementioned studies that only covered several decades at most, this work is the first to use EHSA on a long time scale. Furthermore, we made a methodological breakthrough by using the analysis with a climatological background, which may lay a foundation for further exploration by researchers in related fields.

The structure of this paper is as follows. Data sources and data processing, which include the cyclic division schemes for temperature and precipitation series, and the statistical tools, such as the Global Moran's *I* and EHSA, are introduced in Section 2. Distributions of the hot spots of three kinds of war—all war, the conflict between agriculturalists and pastoralists ("agri-nomadic conflict"), and rebellion under different climatic phases (warm versus cold/wet versus dry) in ancient China are presented in Section 3. Some discussions about the effects of climatic and other non-climatic factors on war hot spots, and our conclusions, are provided in Sections 4 and 5, respectively.

2. Materials and Methods

2.1. Data Source and Data Processing

The data used in this study included climatic series and battle coordinates. The procedures of cycle divisions for temperature and precipitation sequences are stated in detail.

2.1.1. Climate

Derived from Ge et al. [32], the paleotemperature anomalies were reconstructed with the partial least squares regression method based on multi-proxies (lake sediments, stalagmites, historical documents, tree rings, and ice cores) from five regions (northeast, central east, southeast, northwest, and the Tibetan Plateau) of China during 5–1995 CE. Due to the relatively coarse decadal resolution, the data were linearly interpolated into an annual sequence. The original data were smoothed with a five-point fast Fourier transform (FFT) filter to represent the 50-year variation. Similarly, in this study, the FFT filter was set to 50 points (via OriginLab 2018) to obtain the same low-frequency signal.

The paleoprecipitation series during 300 BCE–2000 CE was synthesized by Zhang et al. [15] from 38 document-based single-proxy hydroclimatic datasets at an annual resolution, using the composite plus scale method [33]. This is the first-published long precipitation sequence that spans the past 2000 years on the national scale. A 300-year Butterworth low-pass filter was applied to retrieve the multi-centennial cycle [15]. In this study, the imperial age 1–1911 CE was taken for consistency, and the average of this sequence was calculated to facilitate comparisons.

2.1.2. Division of Climatic Cycles

On the basis of a few criteria, the temperature and precipitation series were divided into different warm–cold and wet–dry cycles.

Temperature: Seven Warm–Cold Cycles

The paleotemperature anomalies reconstructed by Ge et al. [32] were originally divided into four warm (5–200, 551–760, 951–1320, and 1921 CE–present) and cold (201–350, 441–530, 781–950, and 1321–1920 CE) intervals. These do not cover the entire period, as this division scheme does not indicate whether 351–440, 531–550, and 761–780 CE belonged to warm or cold periods. In this study, by referencing the definitions of warm and cold phases from Zhang et al.'s [1] first study on the relationship between climate change, social unrest, and dynastic transition in historical China, the start and end of a warm or cold stage were placed in the midpoint between the highest and lowest temperature anomalies. Based on this criterion, the procedure of cyclic division was as described below:

(1) Determination of the maxima and minima over the temperature sequence: The maximum in 575 CE and minimum in 615 CE were excluded due to the short duration of the resultant warm (530–594 CE) and cold (595–659 CE) periods that lasted for only 65 years. The maximum in 1911 CE was disregarded, as the warm phase in 1873–1911 CE would have been too short to avoid any possible bias otherwise. Another minimum in 95 CE and maximum in 115 CE had a slight difference in temperature anomalies and were not considered. Accordingly, seven pairs of extrema were identified during 5–1911 CE.

(2) Calculation of the midpoint for each pair of extrema: The midpoint from a maximum to a minimum was set as the end of a warm stage, and the year after was treated as the start of a cold phase. By contrast, the midpoint from a minimum to a maximum was set as the end of a cold period, and the year after was treated as the start of a warm stage. The maximum of 1911 CE was excluded in the calculations.

Therefore, seven temperature cycles were defined according to this division scheme (Figure 1a). Each warm and cold phase is listed in Table 1. The duration of all warm periods was 916 years, while cold periods covered 991 years in total. Hence, the warm and cold intervals were relatively balanced compared with the results from Ge et al. [32], in which there were 855 and 1010 years of warm and cold stages, respectively.

Precipitation: Three Wet–Dry Cycles

The paleoprecipitation reconstruction from Zhang et al. [15], which was used to discuss the interactions between agriculturalists and pastoralists in imperial China, was divided into three "Yang" (agriculturalist empires took control of the hinterland) and "Yin" (nomadic tribes invaded and established their own regimes on agricultural region) periods. The Yang–Yin division scheme is actually dynasty-oriented rather than climate-based. Specifically, Yin 1 happened from the Eastern Jin dynasty in 317 CE until the end of the Southern and Northern dynasties in 589 CE, Yin 2 occurred during the Southern Song–Yuan dynasty (1127–1368 CE), and Yin 3 coincided with the Qing dynasty (1644–1911 CE). Here, a new criterion for re-delimiting the precipitation curve was established, in which a wet (dry) phase can be defined when the 300-year smoothed precipitation is above (below) the average of the series (about 666.7 mm/year). Hence, three precipitation cycles were determined, and

over the study period, the lengths of all wet and dry periods lasted for 826 and 1085 years, respectively (Figure 1b and Table 1).

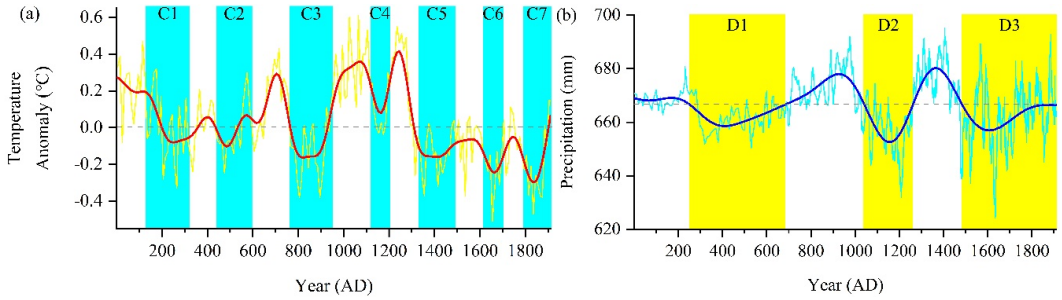

Figure 1. (**a**) Paleotemperature anomaly under the seven-cycle scheme. Note: The annual and 50-year FFT-smoothed series are colored in yellow and red, respectively. Seven cold phases are highlighted in cyan bars. (**b**) Paleoprecipitation reconstruction under the three-cycle scheme. Note: The annual and 300-year curves (smoothed by Butterworth low-pass filter) are shown in cyan and blue, respectively. Three dry intervals are marked by yellow bars.

Table 1. Divisions of warm (W)/cold (C) and wet (W)/dry (D) cycles in ancient China, 1–1911 CE.

Warm Period	Year	Cold Period	Year	Wet Period	Year	Dry Period	Year
W1	5–125	C1	126–320	W1	1–249	D1	250–685
W2	321–440	C2	441–595				
W3	596–765	C3	766–950	W2	686–1041	D2	1042–1262
W4	951–1120	C4	1121–1205				
W5	1206–1330	C5	1331–1490				
W6	1491–1615	C6	1616–1705	W3	1263–1483	D3	1484–1911
W7	1706–1790	C7	1791–1911				

2.1.3. War

War data were gathered from the Tabulation of Wars in Ancient China, an appendix that belongs to the Military History of China, which was summarized by the Editorial Committee of Chinese Military History [34] and has been extensively employed in previous research [1–5,8–10,14–20]. In this study, battle was considered the basic unit of war. The criterion is that if two sides engaging in a war have a fight in reality, then such a fight is regarded as a battle. The terms 'battle' and 'war' are interchangeable in this study when referring to different categories. All the ancient battlefields in this compendium were verified using the Historical Atlas of China [35], counted within the present territory of China, and converted into currently used place names. In other words, battlefields beyond the national boundary were excluded even though they were historically in the areas that belonged to the Chinese Empire. The exclusion of such battlefields may affect the spatial pattern of war, yet these outliers only account for a small proportion of all records—they are usually difficult to locate due to extreme remoteness and the lack of documents. Thus, 5501 battlefields during 1–1911 CE were identified in this study. This number only represents battle locations with definite coordinates, which means the actual number is larger. However, battles do not actually occur at an exact point. From a micro perspective, a battle should have a combat zone, which cannot be measured because people never know much about it. Therefore, the hot spots derived from battle points or coordinates can only be examined in a large framework. The spatial scale of this study was set to national rather than regional and local scales. The definitions of different kinds of wars (i.e., agri-nomadic conflict and rebellion) are provided in Supplementary Materials.

2.2. Methods

In the "Spatial Autocorrelation" tool of ArcMap, the Global Moran's *I* statistic, based on feature locations and attribute values [36], was adopted to measure the degree of global spatial autocorrelation

(or, roughly speaking, to decide whether there was a spatial cluster effect) for different kinds of war in historical China. Before the tool can be applied, a grid containing the point data of battlefields was generated to facilitate the statistical analysis. In this study, 100 km was selected as the length of each square cell (Figure 2, and the reason for this is detailed in Supplementary Materials). Then, the number of battles in each cell of the grid was counted. Next, the Global Moran's I statistic was calculated according to

$$I = \frac{n}{S_0} \frac{\sum_{i=1}^{n} \sum_{j=1}^{n} w_{i \cdot j}(x_i - \overline{x})\left(x_j - \overline{x}\right)}{\sum_{i=1}^{n}(x_i - \overline{x})^2} \quad (1)$$

where n is the total number of cells, x_i and x_j are the counted battle number in cells i and j respectively, $\overline{x}$ is the mean value of battle number in all cells, and $w_{i,j}$ denotes the proximity between i and j. When i and j are adjacent, $w_{i,j} = 1$; otherwise, $w_{i,j} = 0$. S_0 denotes the aggregate of all spatial proximity as

$$S_0 = \sum_{i=1}^{n} \sum_{j=1}^{n} w_{i,j} \quad (2)$$

The z-score for the Global Moran's I statistic is computed as

$$z = \frac{I - \mathrm{E}[I]}{\sqrt{\mathrm{V}[I]}} \quad (3)$$

where E[I] and V[I] are the expectation and variance, respectively, with the formulas

$$\mathrm{E}[I] = -1/(n-1) \quad (4)$$

$$\mathrm{V}[I] = \mathrm{E}[I^2] - \mathrm{E}[I]^2 \quad (5)$$

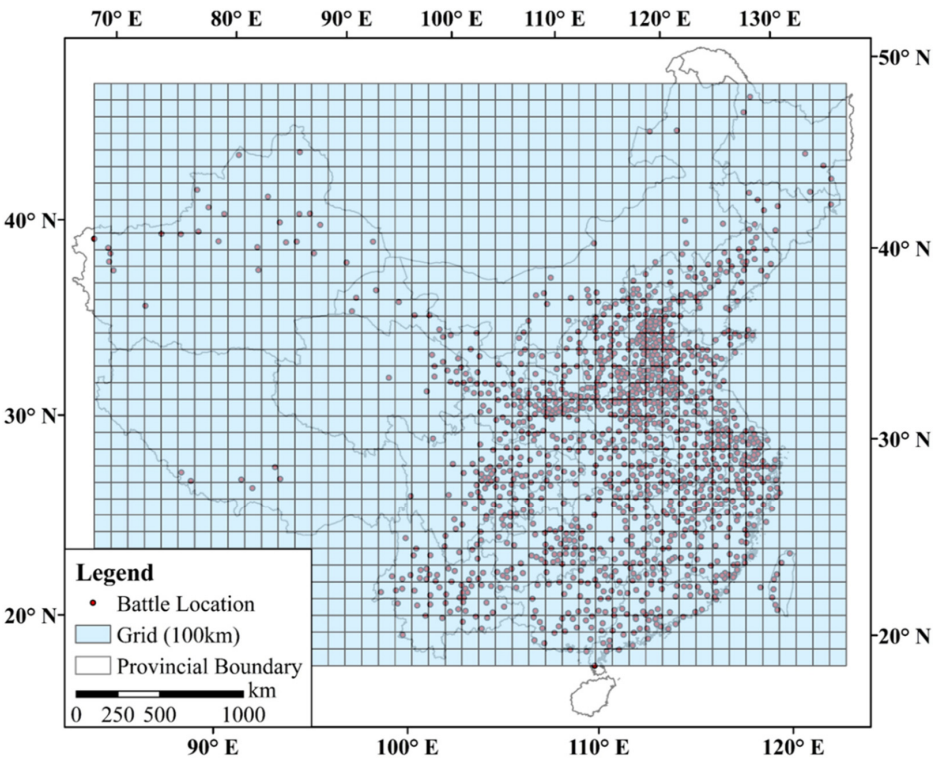

Figure 2. Battle location and the grid (100 × 100 km per cell) adopted in this study.

The index ranges between −1 and 1. The spatial autocorrelation is positive (negative) if the value is larger (smaller) than 0. The higher (lower) the value, the more clustered (dispersed) the war. There is no spatial autocorrelation (i.e., random distribution) when the value is equal to 0.

As the Global Moran's *I* becomes positive, it is possible that there are some hot spots in which battles are clustered in space. Thus, in this research, EHSA was used to visualize the foci of war. The operational procedure of EHSA is realized in two major steps. First, a space–time cube with network common data form (.nc format) was created by running the tool "Create Space Time Cube" in the package "Space Time Pattern Mining Tools" of ArcMap. Instead of real 'points' (e.g., battle coordinates), the hot spots are an array of grids in which point data are aggregated and counted. Each cell (or bin) must have the same size. In this study, 100 km was chosen as the length of the side for each bin, because a bin less than 100 km (e.g., 50 km) would lead to innumerable cells, each of which only covers a small area. In this case, the bin number that contains battlefields may be small, whereas others may be largely blank. By contrast, if the length of the side is more than 100 km (e.g., 200 km), the resultant patterns may be too coarse to decipher, since only limited amounts of bins reside in the study area (Figure S1). Therefore, the medium size of 100 × 100 km was suitable for this task.

During the first step, the Mann–Kendall trend test (or M–K test) was automatically conducted to evaluate the overall trend for all bins in the cube. It is a non-parametric test used to analyze whether data are consistently increasing or decreasing over time [37,38]. More details about the M–K test are provided in Supplementary Materials. Second, the cube was input in the Emerging Hot Spot Analysis tool, and the Getis-Ord *Gi** statistic (i.e., the traditional hot spot analysis) was calculated for each bin. The formula for obtaining the *Gi** is given as [39]

$$G_i^* = \frac{\sum_{j=1}^{n} w_{i,j}x_j - \bar{x}\sum_{j=1}^{n} w_{i,j}}{S\sqrt{\frac{n\sum_{j=1}^{n} w_{i,j}^2 - \left(\sum_{j=1}^{n} w_{i,j}\right)^2}{n-1}}} \quad (6)$$

where

$$\bar{x} = \frac{\sum_{j=1}^{n} x_j}{n} \quad (7)$$

$$S = \sqrt{\frac{\sum_{j=1}^{n} x_j^2}{n} - (\bar{x})^2} \quad (8)$$

Once the analysis was completed, each bin had an associated *z*-score, *p*-value, and hot spot classification. With the resultant trend, *z*-score, as well as *p*-value for each location, the EHSA tool categorized eight kinds of hot spots, which are listed in Table 2.

Table 2. Definitions of various hot spots in EHSA.

Category	Definition
New	The most recent time step interval is hot for the first time.
Consecutive	A single uninterrupted run of hot time step intervals, being comprised of less than 90% of all intervals.
Intensifying	At least 90% of the time step intervals are hot and are becoming hotter through time.
Persistent	At least 90% of the time step intervals are hot, with no trend up or down.
Diminishing	At least 90% of the time step intervals are hot and are becoming less hot over time.
Sporadic	Some of the time step intervals are hot.
Oscillating	Some of the time step intervals are hot, some are cold. The most recent time step interval is hot.
Historical	At least 90% of the time step intervals are hot, but the most recent time step interval is not.

(http://desktop.arcgis.com/en/arcmap/latest/tools/space-time-pattern-mining-toolbox/learnmoreemerging.htm).

In terms of the spatiality of war, EHSA surpasses the traditional hot spot analysis because bins with high frequencies of battles surrounded by high values can be determined and various hot spots are categorized based on the variation trends over time. Accompanying hot spots, however, the spatiotemporal patterns of cold spots (i.e., clusters of low values) are generated, which may be

meaningless since war hot spots were prioritized in this study. Only significant hot spots are presented ($p < 0.05$).

3. Results

3.1. Global Moran's I

The results of the Global Moran's *I* are provided in Table 3. The values ranged between 0.37 and 0.59 and were all significantly positive ($p < 0.01$), which indicates the cluster effect of war (i.e., positive spatial autocorrelation or spatial dependency) and the feasibility of EHSA. In addition, except for agri-nomadic conflict between warm and cold phases, the statistics during all cold and dry intervals were larger than those in warm and wet stages. This illustrates that battles became more concentrated in cold and dry climate, but were slightly scattered in warm and wet conditions. The indexes for all war at any climatic mode were the largest, probably because each cell of the grid contains more battlefields. This is followed by rebellion, and agri-nomadic conflict had the smallest values (except that the value for rebellion in warm periods was the smallest), which means there seems to be a positive correlation between battle number and the degree of the concentration of war.

Table 3. The Global Moran's *I* for three kinds of war in all warm/cold and wet/dry intervals.

Climatic Phase	All War	Agri-Nomadic Conflict	Rebellion
Warm	0.508 **	0.471 **	0.422 **
Cold	0.588 **	0.416 **	0.572 **
Wet	0.487 **	0.373 **	0.457 **
Dry	0.579 **	0.491 **	0.542 **

Note: ** $p < 0.01$.

3.2. Mann–Kendall Trend Test

Table 4 shows that except for wet periods, the hot spots for all war during the other climatic phases failed to pass the M–K test as the trend statistics were insignificant. The statistics for agri-nomadic conflict at any climatic stage were significantly positive compared with those for all war. The value for all warm intervals was the largest (8.446, $p < 0.01$) amongst all statistics. For rebellion, the counterpart of all warm stages failed to pass the M–K test at the level of 0.05, whereas other statistics were positively significant, and the value for wet conditions was the largest (4.075, $p < 0.01$). Thus, the results of the trend test indicate that notwithstanding the difference in climatic phase, the frequencies of agri-nomadic conflict and rebellion in imperial China basically increased through time.

Table 4. Trend statistic for three categories of war during all warm/cold and wet/dry phases

Climatic Phase	All War	Agri-Nomadic Conflict	Rebellion
Warm	0.979	8.446 **	1.548
Cold	−0.596	3.130 **	2.207 *
Wet	4.445 **	3.103 **	4.075 **
Dry	−0.775	6.678 **	3.026 **

Note: ** $p < 0.01$, * $p < 0.05$.

3.3. EHSA Pattern and Explanation

The explanations of the spatial patterns of EHSA involve many geographical names (Figure S2) and historical periods (Table S1) in China. Figure 3a shows that hot spots were preponderantly distributed in northern China, i.e., from the border between Qinghai and Gansu to western Liaoning, during all warm stages. Only a few oscillating hot spots were located in the Yangtze River Delta. Intensifying hot spots indicate that the areas were becoming increasingly hot (i.e., battles were becoming increasingly frequent). They were chiefly concentrated in central Shaanxi–eastern Gansu and southern

Shanxi–the North China Plain and surrounded by other types. Beyond that, the south and north were predominantly occupied by historical versus sporadic and oscillating hot spots, respectively. As historical hot spots are hot most of the time but not hot in the most recent time, this situation implies the alteration of hot spots in history. To the north, probably along the Great Wall, battles were not as frequent as those in intensifying hot spots; therefore, they were categorized as sporadic or oscillating. Similarly, battles were occasionally clustered, but scattered or even absent sometimes in the Yangtze River Delta, which created oscillating hot spots.

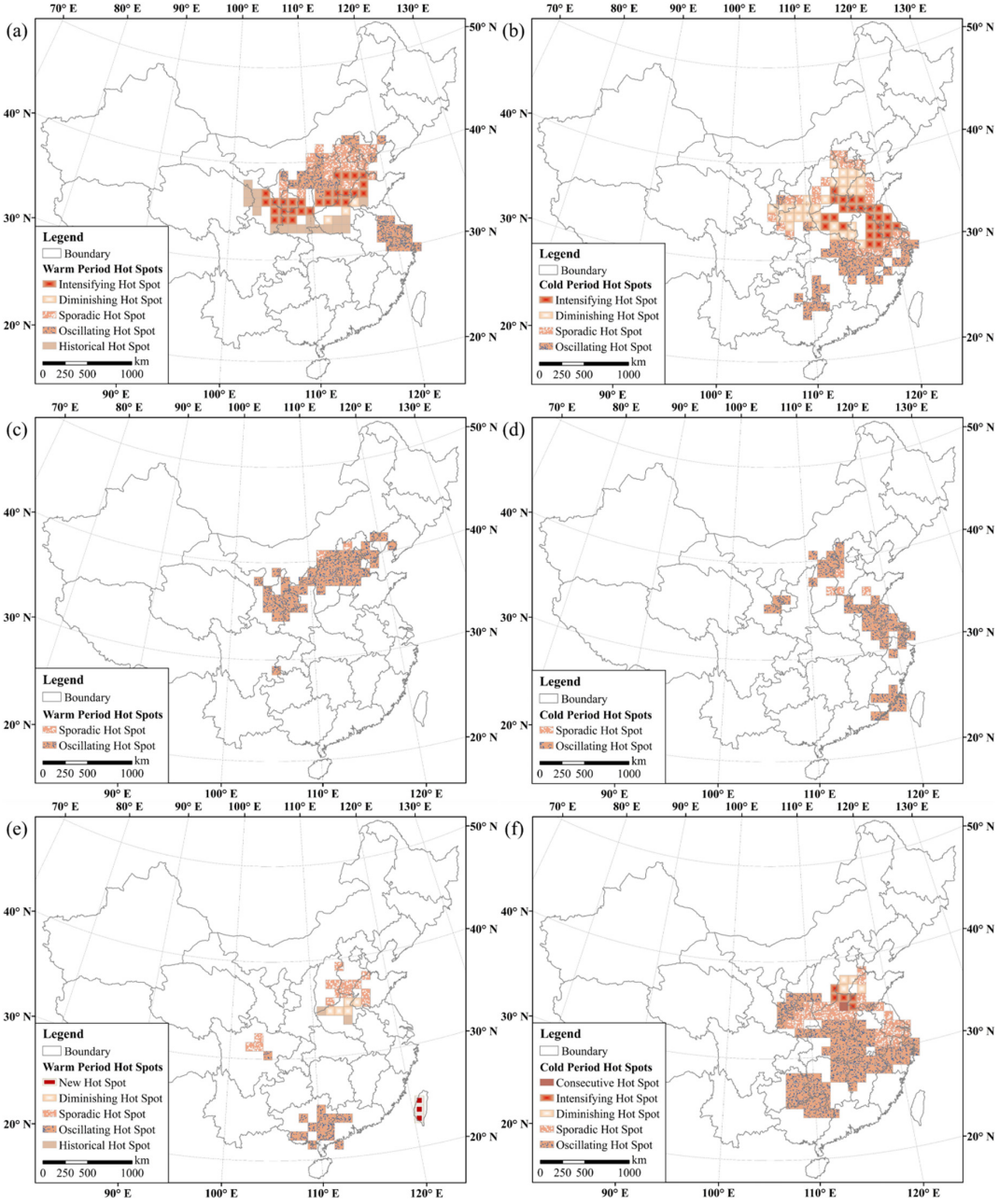

Figure 3. EHSA patterns of all warm and cold periods for three types of war: (**a**,**b**) All war, (**c**,**d**) agri-nomadic conflict, and (**e**,**f**) rebellion. Only significant hot spots ($p < 0.05$) are shown (the same as Figure 4).

By contrast, intensifying hot spots moved massively southeastward to the Central Plain and more prominently to the Jianghuai region and the lower reaches of the Yangtze River during all cold intervals (Figure 3b). The original hot spots in warm periods turned into diminishing hot spots, along with a

few sporadic or oscillating cells in central Shaanxi–eastern Gansu and the North China Plain. Since diminishing hot spots are opposite to intensifying hot spots in nature, this alteration indicates a less hot pattern of war (or less frequent battles) in northern China over time. Furthermore, the hot spots in all cold stages were generally situated farther south/southeast as they disappeared from northeastern Qinghai and central Gansu to the northern Loess Plateau and northern Hebei, whereas they appeared to the south of 30° N in a larger proportion. However, as battles in the middle–lower reaches of the Yangtze River–Yangtze River Delta and near the border of Hunan, Guangxi, and Guizhou were only concentrated during certain intervals, the hot spots in these areas were categorized as oscillating or sporadic.

Figure 3c,d visualize the EHSA patterns for agri-nomadic conflict over all warm and cold stages. In Figure 3c, there were only two sporadic hot spots, while others were oscillating hot spots, extending from central Gansu to western Liaoning. This pattern represents the confrontations between agricultural empires and nomadic tribes/regimes along the Great Wall in historical China. However, when carefully examining the time-series, the conflicts contained by oscillating hot spots were concentrated in two main periods: The Northern Song and Ming dynasties (Table S1). The war against the Liao and Western Xia for the former, and that against the Mongols for the latter, occupied the largest proportion, whereas battles during other stages were not intensive. This result is in line with the definition of oscillating hot spot, i.e., occasionally hot (highly clustered), occasionally cold (sparsely scattered), and the last time step (i.e., in the Ming dynasty) is hot.

In comparison, the hot spots for agri-nomadic conflict in cold climate principally shifted southeastward (Figure 3d). Although some cells remained in northern China, they do not match the scale in warm stages. Instead, hot spots (again prevailingly classified as oscillating) were more concentrated in the Jianghuai region, the lower reaches of the Yangtze River–Yangtze River Delta, and Fujian. Similarly, they are related to the distributions of battles during certain phases. Those in the Jianghuai region and the lower reaches of the Yangtze River–Yangtze River Delta resulted from N–S confrontations, such as northern dynasties versus southern dynasties and Jin versus Southern Song (Table S2). The hot spots in Fujian could be explained by the Ming–Qing war. Given that these oscillating hot spots emerged in different periods, the existence of this category is understandable.

The EHSA patterns for rebellion in all warm and cold stages are depicted in Figure 3e,f. In Figure 3e, the hot spots in all warm periods expanded outward and were clustered in four separate parts: Sichuan, the Central Plain, Taiwan, and Guangxi–Guangdong. Five kinds of hot spots were generated: new, diminishing, sporadic, oscillating, and historical. Historical and diminishing hot spots only emerged in the Central Plain, where rebellions were concentrated in earlier eras but gradually became less frequent. Oscillating hot spots mostly appeared in Guangxi and Guangdong, in which battles largely occurred in later eras but were not dense. Sporadic hot spots were distributed in the Chengdu Plain and its northwest, with a few adjacent to diminishing hot spots in northern China. Battles in these areas were concentrated, yet they were occasionally intensive in some intervals. Finally, the new hot spots in western Taiwan may denote the recent revolts during the Qing dynasty.

The rebellion hot spots in all cold phases were more clustered (Figure 3f). The majority of them were oscillating hot spots, spreading from eastern Guizhou to northern Zhejiang and occupying the middle reaches of the Yangtze River. Another group in the Loess Plateau was adjacent to sporadic hot spots, which extended from Guanzhong to the Central Plain, with another part emerging in the Yangtze River Delta. Other types—such as consecutive, intensifying, and diminishing hot spots—appeared in northern China with a few cells only. Diminishing hot spots were situated north of intensifying hot spots, which implies the southward movement of the war focus through time. A comparison with the warm climate pattern showed that the hot spots in the northern Central Plain (southern North China Plain) changed from diminishing (sporadic) cells in all warm intervals to intensifying–consecutive (diminishing) ones in all cold phases. As a traditional warring zone in ancient China, the northern Central Plain became increasingly hot in recent time steps, particularly during the Ming–Qing transition and the late Qing dynasty. Sporadic hot spots in the Guanzhong–Central Plain and the Yangtze River

Delta were not always hot. To the south, oscillating hot spots primarily included the rebellions during later cold stages, indicating the inward contraction of rebellion in cold periods.

The spatial patterns derived from EHSA during all wet and dry stages are visualized in Figure 4. Figure 4a presents the result of all wet periods for all war. Similar to Figure 3a, four types of hot spots (intensifying, diminishing, sporadic, and oscillating) dominated northern China and stretched from eastern Gansu to the North China Plain via Guanzhong, Shanxi, and the Central Plain. They also spread southeastward to the Jianghuai region, the lower reaches of the Yangtze River, and the Yangtze River Delta, but were exclusively covered by oscillating hot spots. Intensifying hot spots were clustered in most of the North China Plain, where battles became increasingly frequent through time. By contrast, in Guanzhong and the eastern Central Plain, the cells that belonged to diminishing hot spots became gradually less hot or not hot in the end, which implies a possible northward movement of battle over time. A striking contrast was observed between the patterns of all wet and dry stages. In Figure 4b, intensifying hot spots shifted to present-day Jiangsu, while the cells in the north mostly turned into diminishing hot spots. Others, such as sporadic and oscillating hot spots, laid in the north (along 40° N) and south (the lower reaches of the Yangtze River) respectively, with a few historical cells scattered around.

Figure 4c,d present the EHSA patterns for agri-nomadic conflicts in all wet and dry stages. The hot spots during wet periods were all clustered in northern China, i.e., from central Ningxia to eastern Hebei, and included three types: intensifying, sporadic, and oscillating. Oscillating hot spots were mainly distributed in Ningxia, northeastern Gansu, and northern Shaanxi, while intensifying hot spots in the North China Plain were surrounded by sporadic ones. The differences among them may have resulted from the proportions of time steps in three wet phases. Still, most hot spots were found in the north during all dry stages (Figure 4d), but their range elongated outward from two sides. The western end extended into central Gansu, while the eastern end extended into northern Liaoning. A few hot spots appeared in the lower reaches of the Yangtze River, which differentiates the patterns between wet and dry phases. All hot spots in northern China were oscillating, indicating the confrontations between agricultural and nomadic regimes along the Great Wall, which escalated in later times. Sporadic and new hot spots emerged in the lower reaches of the Yangtze River and coastal Fujian, respectively. Hence, the hot spots in southern China represent the southward nomadic invasions, and the new hot spot can be associated with the Manchu conquest during the Ming–Qing transitional period.

The EHSA results for rebellion in all wet and dry intervals are displayed in Figure 4e,f, which are similar to the patterns for all warm and cold stages in Figure 3e,f. The three separate parts in all wet phases indicate that hot spots were clustered in the Central–North China Plain, the lower reaches of the Yangtze River, as well as Guangxi and Guangdong (Figure 4e). The northern part, which was primarily occupied by sporadic hot spots, was surrounded by several oscillating ones, while the latter laid in the eastern and southern parts. For rebellions in sporadic hot spots, there were more time steps during the second wet period, but oscillating hot spots included more battles during the last wet stage. Thus, the hot spots in the north and south presented different patterns. The hot spots during all dry phases were principally concentrated in the lower reaches of the Yangtze River–Yangtze River Delta and expanded southwestward to eastern Guizhou, part of Hunan and Guangxi, along with those from Guanzhong to the Central Plain (Figure 4f). Except for several diminishing hot spots in the north with surrounding sporadic ones, oscillating hot spots dominated the pattern. The difference between sporadic and oscillating hot spots may be attributed to the proportions of time steps in different dry stages. For diminishing hot spots, rebellions were less frequent in later periods, which implies the southward movement of rebellion focus through time.

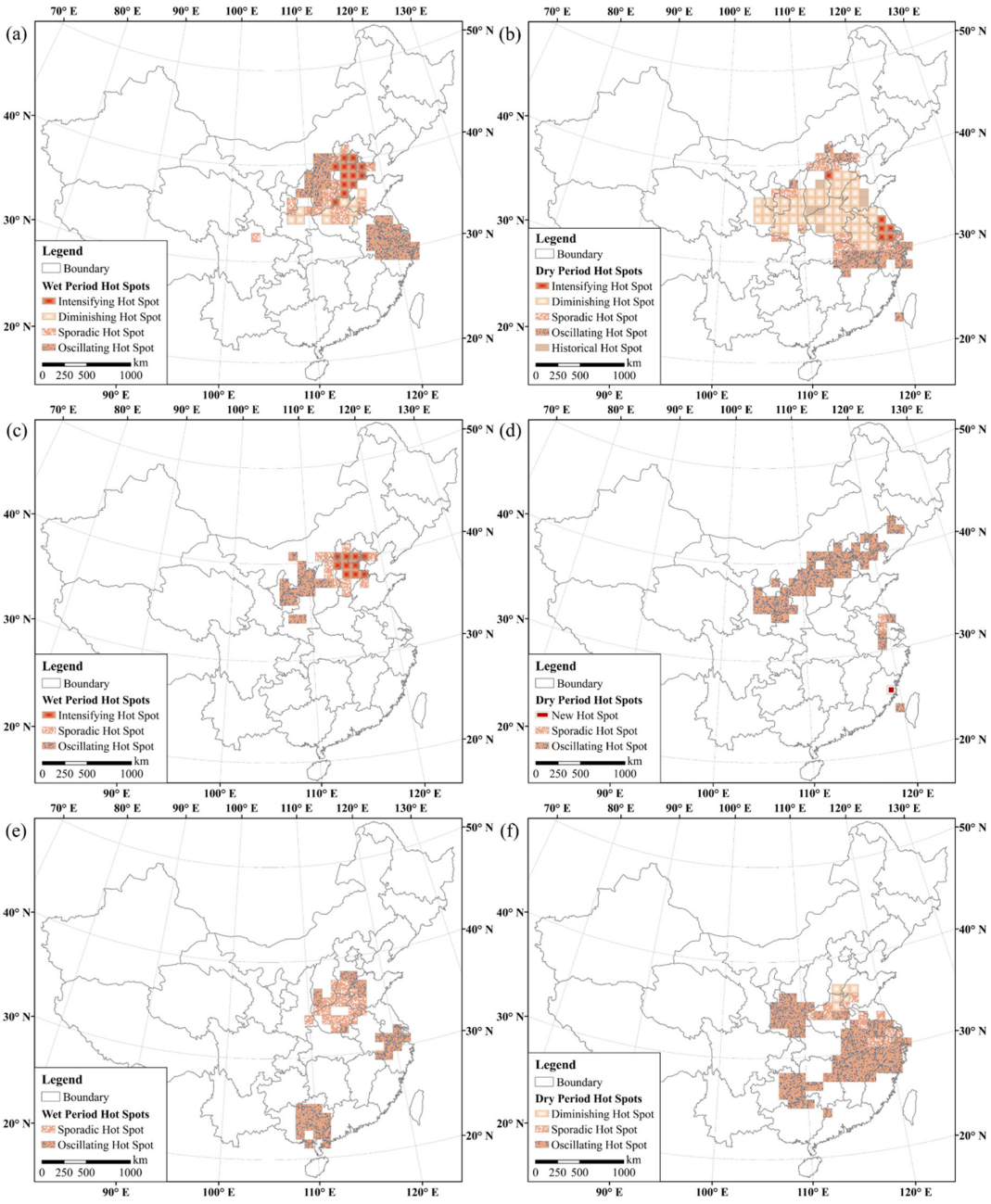

Figure 4. EHSA patterns of all wet and dry stages for three kinds of war. (**a**,**b**) All war, (**c**,**d**) agri-nomadic conflict, and (**e**,**f**) rebellion.

4. Discussion

4.1. Effect of Climate Change on the Hot Spot of War

In this study, we attempted to quantify the cluster effect of war and determine the spatiotemporal pattern of war hot spots in historical China by emphasizing a possible climatological root. On the whole, warm and wet (cold and dry) climate and the accompanying shifts in climatic especially temperature zones, may have brought about the north/west/northwestward (south/east/southeastward) movements of agricultural and pastoral zones. The spatial distributions of war hot spots, particularly the intensifying ones, varied correspondingly. Notably, different from traditional hot spots, those in this research contain temporal information (i.e., time steps/series in each bin). The proportions of time steps of later periods were larger in southern hot spots, which was consistent with the overall decline in

temperature throughout the last two millennia (in particular, during the Little Ice Age (LIA), Figure 1a). In comparison, precipitation fluctuated as cycles without a significant trend (Figure 1b), which shows that the N–S disparities of hot spots may have been more temperature-dependent. The cyclic and long-term temperature variations and the resultant patterns of war hot spots in this work are similar to the findings in Zhang et al. [21], who used the Standard Deviational Ellipse as another spatial analytical tool but for the detection of directional characteristics/differences of war during three secular temperature cycles.

Specifically, as shown by the results in Figures 3 and 4, two categories of war—i.e., agri-nomadic conflict and rebellion, which responded to climate change differently, had different hot spot patterns. First, for agri-nomadic conflict, the strength of agricultural empire rose under warm and wet conditions, so that the central government could either afford expeditions toward Northwest China—i.e., the hinterland of steppes—and maintain control over the nomads there, or at least keep an equilibrium of military power against nomadic tribes/regimes along the borderline. This is why nearly all hot spots of agri-nomadic conflicts were concentrated in the north during such climatic phases. Conversely, cold and dry climate severely affected the economic bases of agricultural empires and nomadic regimes/tribes by reducing grain yields and herding resources, respectively. The weakened power of the central government meant that the military initiative held in warm and/or wet periods gave way to passive frontier defense against nomads [40]. Besides, driven by the cooling- and/or arid-induced environmental degradation, nomads had no choice but to migrate southward, and their conflicts with agriculturalists became increasingly intensive, even breaking through the boundaries and massively invading southward [41,42]. Noticeably, after comparing the patterns between Figures 3d and 4d, we observed many more hot spots in Southeast China during cold intervals than in dry periods, which implied that the effect of temperature on war hot spots may have been stronger than that of precipitation.

Second, with respect to rebellion, similar to the case of agri-nomadic conflict, warm and wet climate typically boosted the economy of agricultural empire, so that the government was able to initiate military campaigns toward the frontier. Moreover, the economic prosperity possibly resulted in rapid population growth, and the demands for expanding living space and relieving the ever-increasing population pressure would have needed to be met. As a result, accompanied by the outward conquest, mass migrations of agriculturalists also occurred during warm and wet intervals, which may have exacerbated the competitions for resources (especially for land) between the Han Chinese and ethnic minorities. Therefore, the emergence and spread of revolts with separate clusters in remote areas, such as the northwest of the Sichuan Basin, Taiwan, Guangdong, and Guangxi, could be interpreted. In comparison, the rebellion hot spots during cold and dry stages shifted inward and widely covered the middle–lower reaches of the Yangtze River, Yangtze River Delta, and the border among Guizhou, Hunan, and Guangxi, but still manifested in the Central Plain and part of the North China Plain, even extending westward to eastern Gansu, as the agricultural base of the Chinese Empire was heavily undermined and the frontier control over ethnic minorities loosened. Nonetheless, the Central Plain remained the core warring zone regardless of climatic phase, yet rebellions somewhat intensified during cold periods.

4.2. Contributions of Other Possible Factors

Our investigation into the linkage between climate and war hot spots does not exclude the possible contributions of other non-climatic factors that mediate the relationship. However, these factors are extremely difficult to spatially quantify from historical documents, in which they are often described ambiguously and fragmented in earlier ages. Yet, such limitations do not interfere with our discussion. Clearly, the hot spots (particularly the intensifying ones) of war overlapped with the developed and populous areas in China, e.g., the Guanzhong Basin, the Central–North China Plain, the Jianghuai region, and the Yangtze River Delta. Hence, this spatial consistency could be interpreted as population-pressure-led social contradiction, an important factor that was observed

before [43–47]. Northern China, where the political center of the Chinese Empire was usually located, greatly benefited from warm and/or wet conditions. The rapid economic development and population growth in such an ecologically fragile agricultural–pastoral transition zone sooner or later deteriorated the environment and caused problems like soil erosion, desertification, and salinization, thereby lowering the land-carrying capacity and triggering resource struggles, and even armed conflict, within the Han Chinese peasants/nomads (e.g., during the Sixteen Kingdoms), or between agriculturalists and pastoralists. Likewise, as northern migrants fled nomadic invasions during cold and/or dry intervals, population increased and the economy flourished in southern China, followed by increasing numbers of conflicts and the emergence of the hot spot zone. Nevertheless, the spatial relationship between war and population/migration in ancient China needs further surveys.

As the agricultural basis in the north was damaged by temperature drops (C5–C7, i.e., the LIA) together with long-term drought (i.e., D3), migration also pointed to the southwest during the late imperial epoch. After the migration from Jiangxi to Huguang in the Ming dynasty, the more massive migration in the Qing dynasty (also known as "Huguang fills Sichuan") boosted the population of the entire southwest, since migrants also flooded into the Yunnan–Guizhou Plateau [48]. Overpopulation on these ecologically fragile mountainous karst landforms exhausted the land-carrying capacity and aggravated the tension between the Han and minorities. Consequently, the hot spots of war were concentrated in these regions. Apart from the population stress resulted from mass migration (sometimes launched by the government), governmental policy may have acted as a catalyst for conflict. For instance, throughout the Ming and Qing dynasties, the management and exploitation of southwestern China deepened. One momentous measure, the bureaucratization of native officers ("Gaitu Guiliu"), aiming at abolishing the hereditary local chieftain system (or "Tusi System") and directly assigning officials by the central government, was implemented. This policy worsened the relationships between the central government and ethnic minorities and ignited numerous revolts in that region. Hence, for rebellion (some were waged by the Miao, Dong, Zhuang, and Yao people), the concentrations of hot spots in the west of the Sichuan Basin, Guangxi, and the Guizhou Plateau could be ascribed to the strengthened rule of the government.

Another possible factor is pertinent to the geopolitical situation. The N–S regime confrontation, which was qualitatively elucidated in previous studies [22,23,49–52], is one of the most pronounced characteristics in Chinese history. It included two aspects: united empires that occupied most of the land area to the south of the Great Wall (China Proper) versus nomadic tribes/regimes that stayed in the steppes of Inner Asia during warm and wet phases, as well as two or more Han Chinese or Han versus nomadic regimes within China Proper during disintegrated eras and also under cold and dry conditions. Looking at Table 1, Table S2, Figure 3b, and Figure 4b, the hot spots (especially the intensifying ones) in the southeast can be partly explained by the latter aspect. Under the circumstances, battles were dominantly clustered in the vicinity of regime borders, or distributed along natural boundaries, such as the Yellow River (e.g., Northern Wei versus Liu Song during the Southern and Northern dynasties), the Qinling Mountains–Huai River (e.g., Wei versus Shu and Wu in the Three Kingdoms Period and Jin versus Southern Song), or farther south, the Yangtze River (e.g., Sui versus Chen).

5. Conclusions

This study is the first attempt to probe into long-term climate change (warm/wet versus cold/dry) and its association with the hot spots of different types of war (all war, agri-nomadic conflict, and rebellion) in imperial China. Looking at the connection from a spatiotemporal perspective with the aid of a few quantitative and visualization techniques, we conclude the following:

1. The cluster effect of war in ancient China was quantified by using the Global Moran's *I*, i.e., cells with large battle numbers tended to concentrate adjacently.
2. The Mann–Kendall trend test showed that, at any climatic mode, agri-nomadic conflict and rebellion basically increased over time, whereas the results for all war were almost insignificant.

3. Regarding EHSA, the hot spots for all war shifted northward and westward during warm and wet intervals, but toward the southeast in cold and dry conditions. For agri-nomadic conflict, hot spots were distributed along the boundary between agricultural and pastoral regimes in warm and wet phases, but reached as far as South China (due to nomadic invasions) during cold and dry stages. For rebellion, with the vicissitude of the Chinese Empire, hot spots spread outward in three to four groups in warm and wet climate but contracted inward during cold and dry periods.
4. EHSA satisfactorily reflected the pattern of war hot spots, on which temperature may have exerted more effect than precipitation.

Supplementary Materials: The following are available online at http://www.mdpi.com/2073-4433/11/4/378/s1, Figure S1: Comparisons of battle number counted within the grids of (a) 50 km, (b) 100 km, and (c) 200 km for each side of a cell, Figure S2: Geographical features of China mentioned in the main text, Table S1: History of China in the study period, Table S2a: N–S confrontation within China Proper during warm and cold phase, 5–1911 CE, Table S2b: N–S confrontation within China Proper during wet and dry phase, 1–1911 CE, Table S3: The Global Moran's *I* for different categories of war and climatic stages based on the grids of 50, 100, and 200 km.

Author Contributions: Conceptualization, D.D.Z.; Data curation, S.Z. and D.D.Z.; Formal analysis, S.Z.; Funding acquisition, D.D.Z.; Investigation, S.Z.; Methodology, S.Z. and D.D.Z.; Project administration, D.D.Z.; Resources, D.D.Z.; Supervision, D.D.Z. and J.L.; Validation, S.Z., D.D.Z., and J.L.; Visualization, S.Z.; Writing—original draft, S.Z.; Writing—review and editing, S.Z., D.D.Z., and J.L. All authors have read and agreed to the published version of the manuscript.

Funding: This research was funded by the Fund for Key Platform Construction Project–Special Project of High Level University Construction at Guangzhou University, grant number 290020363.

Acknowledgments: The authors thank the anonymous reviewers for their valuable comments on this manuscript.

Conflicts of Interest: The authors declare no conflict of interest.

References

1. Zhang, D.; Jim, C.; Lin, C.; He, Y.; Lee, F. Climate change, social unrest and dynastic transition in ancient China. *Chin. Sci. Bull.* **2005**, *50*, 137–144. [CrossRef]
2. Zhang, D.D.; Jim, C.Y.; Lin, G.C.; He, Y.; Wang, J.J.; Lee, H.F. Climatic change, wars and dynastic cycles in China over the last millennium. *Clim. Chang.* **2006**, *76*, 459–477. [CrossRef]
3. Zhang, D.D.; Zhang, J.; Lee, H.F.; He, Y. Climate change and war frequency in eastern China over the last millennium. *Hum. Ecol.* **2007**, *35*, 403–414. [CrossRef]
4. Lee, H.F.; Zhang, D.D. Changes in climate and secular population cycles in China, 1000 CE to 1911. *Clim. Res.* **2010**, *42*, 235–246. [CrossRef]
5. Zhang, D.D.; Lee, H.F. Climate change, food shortage and war: A quantitative case study in China during 1500–1800. *Catrina* **2010**, *5*, 63–71.
6. Zhang, Z.; Tian, H.; Cazelles, B.; Kausrud, K.L.; Bräuning, A.; Guo, F.; Stenseth, N.C. Periodic climate cooling enhanced natural disasters and wars in China during AD 10–1900. *Proc. R. Soc. B* **2010**, *277*, 3745–3753. [CrossRef]
7. Bai, Y.; Kung, J.K.S. Climate shocks and Sino-nomadic conflict. *Rev. Econ. Stat.* **2011**, *93*, 970–981. [CrossRef]
8. Lee, H.F.; Zhang, D.D. A tale of two population crises in recent Chinese history. *Clim. Chang.* **2013**, *116*, 285–308. [CrossRef]
9. Lee, H.F. Climate-induced agricultural shrinkage and overpopulation in late imperial China. *Clim. Res.* **2014**, *59*, 229–242. [CrossRef]
10. Pei, Q.; Zhang, D.D. Long-term relationship between climate change and nomadic migration in historical China. *Ecol. Soc.* **2014**, *19*, 68. [CrossRef]
11. Zheng, J.; Xiao, L.; Fang, X.; Hao, Z.; Ge, Q.; Li, B. How climate change impacted the collapse of the Ming dynasty. *Clim. Chang.* **2014**, *127*, 169–182. [CrossRef]
12. Fang, X.; Su, Y.; Yin, J.; Teng, J. Transmission of climate change impacts from temperature change to grain harvests, famines and peasant uprisings in the historical China. *Sci. China Earth Sci.* **2015**, *58*, 1427–1439. [CrossRef]

13. Xiao, L.; Fang, X.; Zheng, J.; Zhao, W. Famine, migration and war: Comparison of climate change impacts and social responses in North China between the late Ming and late Qing dynasties. *Holocene* **2015**, *25*, 900–910. [CrossRef]
14. Zhang, D.D.; Pei, Q. Gone with winds: A quantitative analysis of battlefield locations and climate shifts in imperial China. In *Geo-Strategy and War: Enduring Lessons for Australian Army*; Dennis, P., Ed.; Big Sky Publishing: Newport, NSW, Australia, 2015; pp. 193–211.
15. Zhang, D.D.; Pei, Q.; Lee, H.F.; Zhang, J.; Chang, C.Q.; Li, B.; Li, J.; Zhang, X. The pulse of imperial China: A quantitative analysis of long-term geopolitical and climatic cycles. *Glob. Ecol. Biogeogr.* **2015**, *24*, 87–96. [CrossRef]
16. Lee, H.F.; Zhang, D.D.; Pei, Q.; Jia, X.; Yue, R.P. Demographic impact of climate change on northwestern China in the late imperial era. *Quat. Int.* **2016**, *425*, 237–247. [CrossRef]
17. Liu, L.; Su, Y.; Fang, X. Wars between farming and nomadic groups from Western Han dynasty to Qing dynasty in north China and relationship with temperature change. *J. Beijing Normal Univ. (Nat. Sci.)* **2016**, *52*, 450–457, (In Chinese with English abstract).
18. Lee, H.F.; Zhang, D.D.; Pei, Q.; Jia, X.; Yue, R.P. Quantitative analysis of the impact of droughts and floods on internal wars in China over the last 500 years. *Sci. China Earth Sci.* **2017**, *60*, 2078–2088. [CrossRef]
19. Pei, Q.; Lee, H.F.; Zhang, D.D. Long-term association between climate change and agriculturalists' migration in historical China. *Holocene* **2017**, *28*, 208–216. [CrossRef]
20. Zhang, S.; Zhang, D.D. Population-influenced spatiotemporal pattern of natural disaster and social crisis in China, AD1–1910. *Sci. China Earth Sci.* **2019**, *62*, 1138–1150. [CrossRef]
21. Zhang, S.; Zhang, D.D.; Li, J.; Pei, Q. Secular temperature variations and the spatial disparities of war in historical China. *Clim. Chang.* **2020**. [CrossRef]
22. Song, J. The geographical pivot of war in ancient China. *J. Cap. Normal Univ. (Soc. Sci. Ed.)* **1994**, *4*, 1–10. (In Chinese)
23. Rao, S. *Layout of the World: General Situation of Military Geography in Ancient China*; People's Liberation Army Press: Beijing, China, 2002. (In Chinese)
24. Wang, X. Spatial distribution and focus area transfer of war and battle in poems of the early-prosperous Tang dynasty. *Data Cult. Educ.* **2009**, *18*, 16–18. (In Chinese)
25. Leng, H. Research on the Transfer of the Northern Border Trouble in Ancient China from Qin and Han to Ming Dynasties. Master's Thesis, Liaoning University, Shenyang, China, May 2011.
26. Zhu, Y.; Newsam, S. Spatio-temporal sentiment hotspot detection using geotagged photos. In Proceedings of the 24th ACM SIGSPATIAL International Conference on Advances in Geographic Information Systems, Burlingame, CA, USA, 31 October–3 November 2016; ACM: New York, NY, USA, 2016. [CrossRef]
27. Sadler, R.C.; Pizarro, J.; Turchan, B.; Gasteyer, S.P.; McGarrell, E.F. Exploring the spatial-temporal relationships between a community greening program and neighborhood rates of crime. *Appl. Geogr.* **2017**, *83*, 13–26. [CrossRef]
28. Coyan, J.A.; Zientek, M.L.; Mihalasky, M.J. Spatiotemporal analysis of changes in lode mining claims around the McDermitt Caldera, northern Nevada and southern Oregon. *Nat. Resour. Res.* **2017**, *26*, 319–337. [CrossRef]
29. Hosseini, S.M.; Parvin, M.; Bahrami, M.; Karami, M.; Olfatifar, M. Pattern mining analysis of pulmonary TB cases in Hamadan Province: Using space-time cube. *Int. J. Epidemiol. Res.* **2017**, *4*, 111–117.
30. Bunting, R.J.; Chang, O.Y.; Cowen, C.; Hankins, R.; Langston, S.; Warner, A.; Yang, X.; Louderback, E.R.; Sen Roy, S. Spatial patterns of larceny and aggravated assault in Miami-Dade County, 2007–2015. *Prof. Geogr.* **2017**, *70*, 34–46. [CrossRef]
31. Harris, N.L.; Goldman, E.; Gabris, C.; Nordling, J.; Minnemeyer, S.; Ansari, S.; Lippmann, M.; Bennett, L.; Raad, M.; Hansen, M.; et al. Using spatial statistics to identify emerging hot spots of forest loss. *Environ. Res. Lett.* **2017**, *12*, 024012. [CrossRef]
32. Ge, Q.; Hao, Z.; Zheng, J.; Shao, X. Temperature changes over the past 2000 yr in China and comparison with the Northern Hemisphere. *Clim. Past.* **2013**, *9*, 1153–1160. [CrossRef]
33. Mann, M.E.; Zhang, Z.; Hughes, M.K.; Bradley, R.S.; Miller, S.K.; Rutherford, S.; Ni, F. Proxy-based reconstructions of hemispheric and global surface temperature variations over the past two millennia. *Proc. Natl. Acad. Sci. USA* **2008**, *105*, 13252–13257. [CrossRef]

34. Editorial Committee of Chinese Military History. *Tabulation of Wars in Ancient China*; People's Liberation Army Press: Beijing, China, 1985. (In Chinese)
35. Tan, Q. *Historical Atlas of China*; SinoMaps Press: Beijing, China, 1982. (In Chinese)
36. How Spatial Autocorrelation (Global Moran's *I*) Works. Available online: https://desktop.arcgis.com/en/arcmap/latest/tools/spatial-statistics-toolbox/h-how-spatial-autocorrelation-moran-s-i-spatial-st.htm (accessed on 26 August 2019).
37. Mann, H.B. Nonparametric tests against trend. *Econometrica* **1945**, *13*, 245–259. [CrossRef]
38. Kendall, M.G.; Gibbons, J.D. *Rank Correlation Methods*, 5th ed.; Griffin: London, UK, 1990.
39. How Hot Spot Analysis (Getis-Ord *Gi**) Works. Available online: https://desktop.arcgis.com/en/arcmap/latest/tools/spatial-statistics-toolbox/h-how-hot-spot-analysis-getis-ord-gi-spatial-stati.htm (accessed on 26 August 2019).
40. Wang, X.; Chen, F.; Zhang, J.; Yang, Y.; Li, J.; Hasi, E.; Zhang, C.; Xia, D. Climate, desertification and the rise and collapse of China's historical dynasties. *Hum. Ecol.* **2010**, *38*, 157–172. [CrossRef]
41. Fang, J. The impacts of climatic change on the Chinese migrations in historical times. *Geogr. Environ. Res.* **1989**, *1*, 39–46, (In Chinese with English abstract).
42. Wang, H. The relationship between the migrating south of the nomadic nationalities in north China and the climatic changes. *Sci. Geogr. Sin.* **1996**, *16*, 274–279, (In Chinese with English abstract).
43. Ho, P.T. *Studies on the Population of China, 1368–1953*; Harvard University Press: Cambridge, MA, USA, 1959.
44. Webster, D. Warfare and evolution of state—reconsideration. *Am. Antiq.* **1975**, *40*, 464–470. [CrossRef]
45. Zhao, W.; Xie, S. *History of Chinese Population*; People's Press: Beijing, China, 1988. (In Chinese)
46. Carneiro, R.L. The transition from quantity to quality: A neglected causal mechanism in accounting for social evolution. *Proc. Natl. Acad. Sci. USA* **2000**, *97*, 12926–12931. [CrossRef]
47. Lee, H.F.; Fok, L.; Zhang, D.D. Climatic change and Chinese population growth dynamics over the last millennium. *Clim. Chang.* **2008**, *88*, 131–156. [CrossRef]
48. Yang, Y. Migration and frontier society: Regulation of the Han-minority contradiction in Yunnan–Guizhou region during the Qing dynasty under the perspective of social control. *J. Yunnan Normal Univ. (Humanit. Soc. Sci.)* **2017**, *49*, 9–19. (In Chinese)
49. Shi, N. Discussion about the situations of west–east and north–south confrontations in historical China. *J. Chin. Hist. Geogr.* **1992**, *1*, 57–112. (In Chinese)
50. Hu, A. *Place with Strategic Importance: An Outline of Military Geography in Historical China*; Hehai University Press: Nanjing, China, 1996. (In Chinese)
51. Yao, X. A brief discussion on the evolution of the spatial orientation of war in ancient China. *Mil. Hist.* **2007**, *4*, 58–60. (In Chinese)
52. Yao, X. Study on the geopolitical model of wars in ancient Chinese dynasties. *Hum. Geogr.* **2007**, *1*, 125–128, (In Chinese with English abstract).